energies

MDPI

Article

Numerical Study on Liquid-Return Characteristics in the Accumulator of the R290 Rotary Compressor

Jie Lin [1,*], Nini Guo [1], Jianhua Wu [2], Liangkun Hong [3] and Jianjiang Jiang [3]

[1] Key Laboratory of Air-Driven Equipment Technology of Zhejiang Province, College of Mechanical Engineering, Quzhou University, Quzhou 324000, China; nnguo@qzc.edu.cn
[2] School of Energy and Power Engineering, Xi'an Jiaotong University, Xi'an 710049, China; wujianhua@mail.xjtu.edu.cn
[3] Hongwuhuan Group Co., Ltd., Quzhou 324000, China; hongliangkun@hongwuhuan.com (L.H.); jiangjianjiang@hongwuhuan.com (J.J.)
* Correspondence: jielin1031@outlook.com; Tel.: +86-15-257-038-716

Abstract: Liquid often exists in the accumulator of the rotary compressor during the process of startup or defrost of air-conditioning systems. Too much liquid entering the compressor cylinder would result in excessive pressure caused by the liquid compression, which is a great threat to the compressor. The liquid return through the liquid-return hole is the key to ensure the stable operation of the compressor. In this paper, the liquid-return characteristics in the liquid-return holes of the accumulator, including the mass-flow rate, liquid velocity and pressure difference between the liquid-return holes, during the startup process of the R290 rotary compressor are numerically investigated. The numerical simulation using the fluent volume of fluid (VOF) method was experimentally validated with the error of 1.55%. The comparison of liquid-return characteristics using different refrigerants is conducted. Effects of refrigerant solubility in the oil, refrigerant/oil-mixture type, liquid-return-hole diameter and compressor frequency on the liquid-return characteristics and liquid shape trough the liquid-return hole are discussed. The results show that the surface tension and viscosity of the liquid are the main factors affecting the liquid-return speed. The liquid-return rate of the refrigerant R290 is slower than that of other refrigerants R22 and R410A. The liquid-return rate increases with the increase in the compressor frequency. We conclude that for air-conditioning systems using R290 as refrigerant, increasing the number of return holes or the hole diameter is necessary to improve the liquid-return characteristics of the compressor. This research will provide theoretical guidance for the optimization of liquid return of rotary compressors using new refrigerants.

Keywords: rotary compressor; liquid return; accumulator; R290

Citation: Lin, J.; Guo, N.; Wu, J.; Hong, L.; Jiang, J. Numerical Study on Liquid-Return Characteristics in the Accumulator of the R290 Rotary Compressor. *Energies* **2022**, *15*, 2469. https://doi.org/10.3390/en15072469

Academic Editor: Adélio Rodrigues Gaspar

Received: 2 March 2022
Accepted: 25 March 2022
Published: 28 March 2022

1. Introduction

Rotary compressors are widely used in variety of home appliances such as air-conditioning systems, heat-pump water heaters, clothes dryers, dehumidifiers and other refrigeration fields. The accumulator, also named the liquid–gas separator, located before the compressor shell, is an important component of a rotary compressor. The primary function of the accumulator is to control excess liquid of refrigerant or oil, preventing liquid compression in the compressor cylinder. It also has the functions of filtering contaminants and acting as an acoustic suction muffler [1,2]. Therefore, the accumulator plays an important role in the performance and reliability of the rotary compressor and its air-conditioning system [3].

Under some circumstances, vapor–liquid two-phase fluid in the compressor accumulator is inevitable. For example, during the startup or defrosting process of the air-conditioning system, a large amount of refrigerant/oil liquid flows into the compressor accumulator from the evaporator [4]. Except for a small amount of refrigerant evaporation, most liquid in the accumulator flows into the compressor cylinder via the liquid-return

hole in the accumulator. The excessive liquid in the accumulator would not only reduce the performance of the air-conditioning due to a lack of refrigerant in the system [5], but also may damage the compressor because of the excessive pressure caused by the liquid compressor [6,7].

In order to improve the liquid-return capacity of the compressor, much work has been carried out on the optimization of the accumulator structure. Feng [8] proposed a novel regeneration accumulator, which effectively enhances the liquid refrigerant's evaporating speed in accumulator and recovers the lost cooling energy in the accumulator. Kang [9] used the accumulator heat exchanger, consisting of an accumulator and an inner heat exchanger, before the compressor in an air conditioner to obtain high system reliability and performance by providing liquid refrigerant to the expansion valve and preventing liquid slugging in the compressor. Because the excess liquid storage of the accumulator is limited, Yun [3] changed the structure of the accumulator to increase the accumulator's liquid storage and the system's refrigerant charge mass, so as to ensure the reliability of the rotary compressor. To improve the liquid separation capacity and optimize the accumulator structure, some studies have been carried out by establishing a two-phase steady-state 1D model of the accumulator in the vehicle's air-conditioning. The relationship between the height of the liquid-return hole, the liquid level and suction-gas fraction are obtained by solving the governing equations [10,11]. This method does not consider the quality of the liquid entering the suction pipe and the phase change of the refrigerant in the accumulator, resulting in a relatively large error. Through CFD simulation, Hrnjak [12] studied the flow characteristics of the two-phase refrigerant/oil mixture in the accumulator of a CO_2 heat-pump system using scroll compressors and analyzed the impact of the oil-bleed-hole size on the liquid level and local pressure drop. The volume of fluid model was used to track the liquid–vapor interface. For the new refrigerant used in the air-conditioning system, the original accumulator structure may cause some problems, because of the special physical properties of the oil and refrigerant. Zheng [13] experimentally founded that for the R32 refrigeration system, within a certain range, the increase in the diameter of the liquid-return hole can significantly increase the cooling capacity and EER. This actually reduces the suction-gas fraction and discharge temperature, thereby improving efficiency.

Except for the evaporation of some liquid refrigerant, most flows out of the accumulator through the liquid-return hole. A big liquid-return hole may result in much liquid entering the compressor cylinder, increasing the risk of compressor damage due to liquid compression [14]. On the other hand, a small liquid-return hole may lead to a lot of refrigerant and oil collected in the accumulator during the startup of the air-conditioning system, which not only prolongs the startup time of the refrigeration system and decreases the suction pressure [15], but also reduces the oil in the compressor and exacerbates the wear.

Overall, much research has been conducted on the improvement of the liquid return of the rotary compressor by experimental or simple simulation methods. However, the liquid-return characteristics, such as the vapor–liquid two-phase flow pattern, local pressure drop and the effect factors inside the accumulator of the rotary compressor are rare in the open literature. Moreover, there are inadequate data for the design of the compressor using an alternative refrigerant in the air-conditioning system, such as R290. In this paper, the liquid-return characteristics in the accumulator during the startup of the rotary compressor are numerically simulated using the fluent volume of fluid (VOF) method. The simulation results are experimentally validated by using the refrigerant R290. The influence of refrigerant solubility in the oil, refrigerant/oil types, liquid-return-hole diameter and compressor frequency on the liquid-return rate and liquid-return-hole droplet shape are discussed. The research will provide theoretical guidance for the design of the rotary compressor using an alternative refrigerant to improve the low liquid-return rate and suction pressure of the air-conditioning system.

2. Modeling

Figure 1 shows the schematic diagram of a two-cylinder rotary compressor. It mainly consists of an accumulator, a shell, a motor, a crankshaft, two bearings, two cylinders and some other components. Refrigerant of low temperature and pressure is sucked into the cylinders through the accumulator. Then, the refrigerant vapor is compressed to a high temperature and high pressure is discharged from the cylinder into the shell through the muffler. After cooling the motor, refrigerant flows out of the shell and into the system through the outlet pipe.

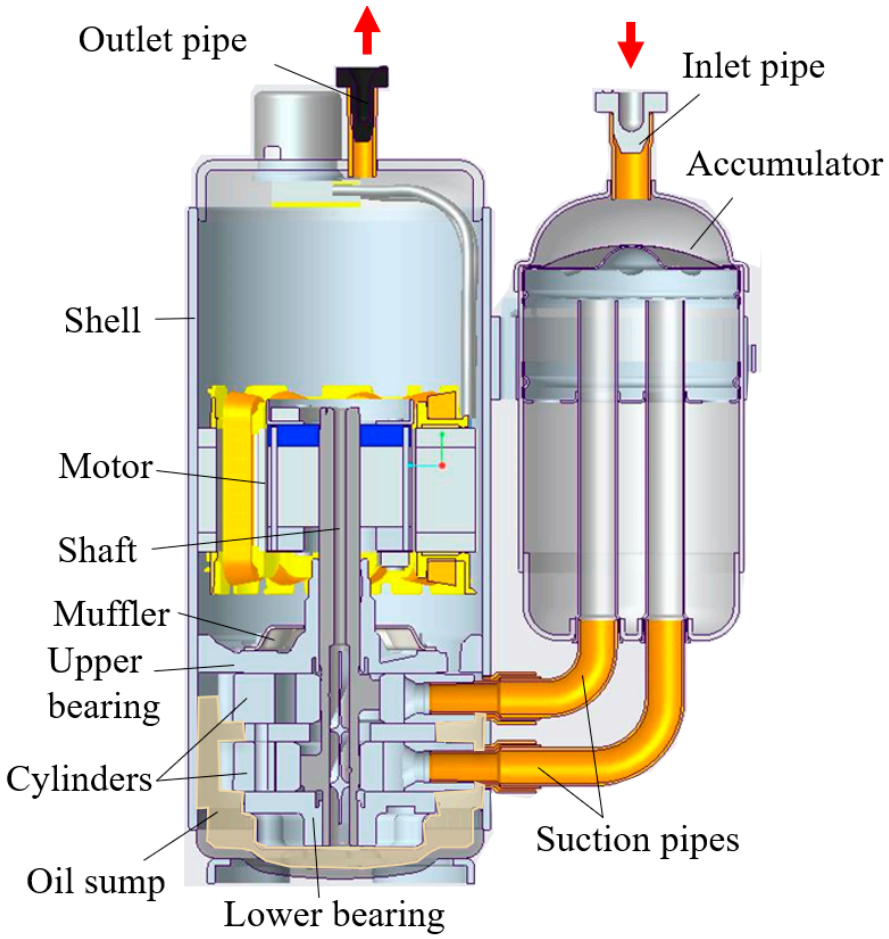

Figure 1. Schematic diagram of the rotary compressor.

To reduce the suction noise and prevent excess liquid refrigerant or oil from going directly into the cylinder during the startup or other operating conditions of the compressor, an accumulator is installed before the shell. The structure and liquid-return capacity of the accumulator have great influence on the performance and reliability of the rotary compressor. Therefore, investigation on the liquid-return characteristics in the accumulator during the startup is conducted in this paper.

2.1. Physical Model and Meshing

Figure 2 shows the geometry model of the accumulator, which is mainly composed of six parts: an inlet pipe, an accumulator shell, liquid-return holes, suction pipes, a screen holder and a tube holder. We extract the fluid domain from the solid domain to calculate the flow characteristics of the oil and refrigerant mixtures.

ANSYS ICEM is used to discrete and mesh the computational domain. The computational grid is shown in Figure 3. To simplify the calculation and make the computation grid more structured, some unimportant chamfers and grooves in the accumulator are ignored.

The grids of irregular parts in the accumulator, such as the upper shell and holders, are unstructured. Grids of other parts, such as the inlet pipe, liquid-return holes and suction pipes and the middle and lower shell are structured. To reduce the number of grids and improve the calculation accuracy, the accumulator is divided into nine blocks.

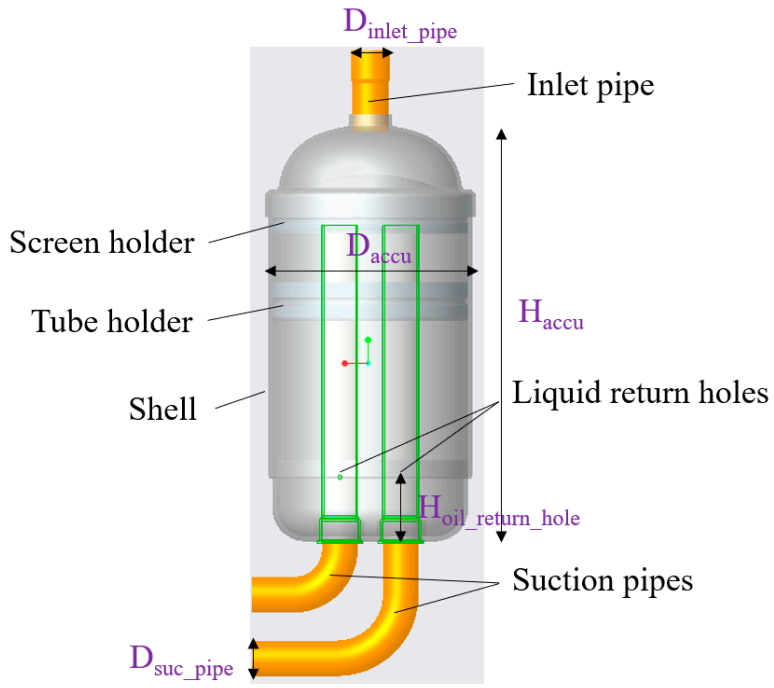

Figure 2. Geometry model of the accumulator.

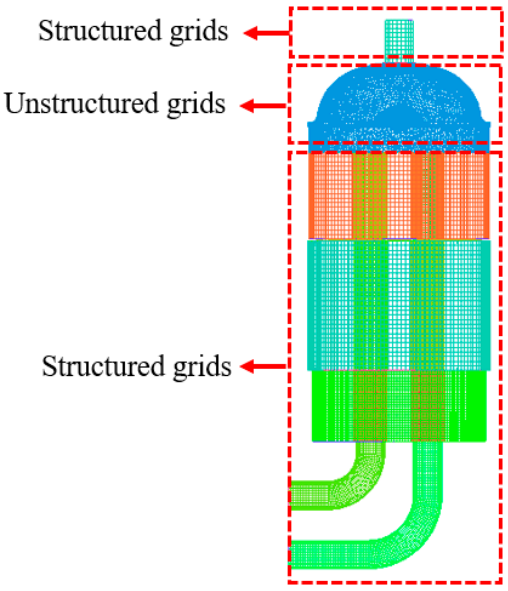

Figure 3. Computational grid.

The grid-independence verification to calculate the mass-flow rate in the liquid-return hole is shown in Figure 4. The number of 680k elements is considered a good choice to balance computational accuracy and computation cost. The size of the suction pipes and the lower part of the accumulator is set as 1 mm. The size of the liquid-return holes is 0.5 mm and the rest are 2 mm. After local adjustment, the minimum quality of the structured grid is 0.508 in the liquid-return hole and the minimum quality of unstructured grids is above

0.358. This structured mesh and high mesh quality can ensure the calculation accuracy at the interface.

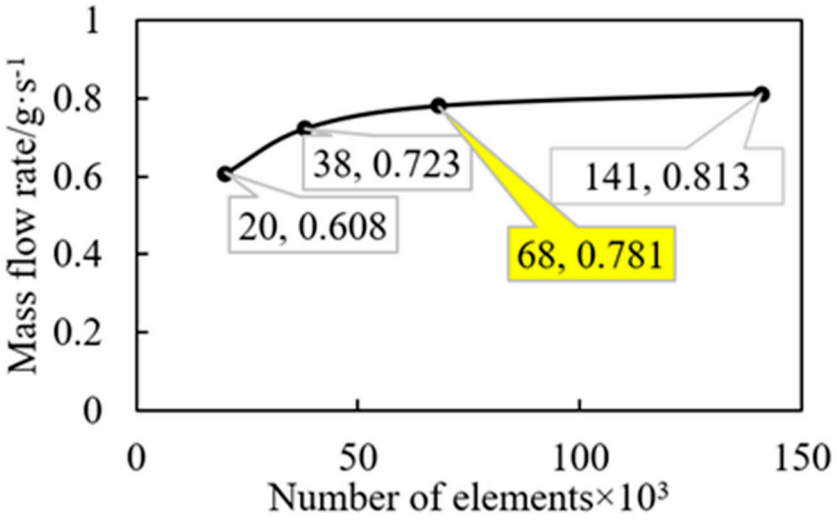

Figure 4. Grid-independence verification.

The structural parameters of the accumulator used in the simulation are shown in Table 1.

Table 1. Structural parameters of the accumulator.

Parameter	D_{accu}/mm	D_{suc_pipe}/mm	$D_{Oil\_return\_hole}$/mm	D_{inlet_pipe}/mm	$H_{oil\_return\_hole}$/mm	H_{accu}/mm
Values	73	12.4	1.5	11.6	22.8	160

2.2. Boundary Conditions and Initial Conditions

2.2.1. Inlet of the Accumulator

The inlet pipe of the accumulator is connected to the outlet of the evaporator. Compared with the great pressure variation in the compressor cylinder, the transient pressure at the evaporator outlet can be considered constant. Therefore, the boundary condition at the accumulator inlet is set as a constant-pressure condition, which can be obtained from the experimental data.

2.2.2. Outlet of the Accumulator

The suction pipes are connected to the cylinder of the compressor (see Figure 1). The volume of the compression chamber in the cylinder changes with the rotation of crankshaft, which causes the continuous change of the volume flow rate of refrigerant in the suction pipe. Compared with the great pressure change in the suction pipes, pressure in the accumulator changes little, so the refrigerant density in the accumulator can be considered constant. Therefore, the boundary condition at the accumulator outlet is set as a variable-velocity condition. The outlet velocity is calculated from the cylinder-volume-change rate, volume efficiency and the suction-pipe-outlet area:

$$u_s = \eta_v \frac{dV/dt}{A_s} \tag{1}$$

where u_s is the outlet velocity of refrigerant in the suction pipe; η_v is the volume efficiency of the compressor; dV/dt is the cylinder-volume-change rate; A_s is the area of the suction-pipe outlet.

The volume-change rate of the compression chamber in the cylinder can be expressed as [16]:

$$\frac{dV}{dt} = \omega[\frac{1}{2}(2-\varepsilon) - (1-\varepsilon)\cos\theta - \frac{1}{2}\varepsilon\cos(2\theta)]{R_c}^2 h_c \varepsilon \quad (2)$$

where ω is the angular velocity of the crankshaft; ε is the crankshaft eccentricity; θ is the crank angle of the crankshaft; R_c and h_c are the radius and height of the cylinder, respectively.

The interpreted UDF is used to implement variable-outlet-velocity condition in the paper.

2.2.3. Initial Conditions

Initially, the lower part of the accumulator is filled with the mixed liquid of refrigerant and oil. The upper part is filled with refrigerant gas. The liquid level is given according to the experiment data, which corresponds to the calculation. Due to the small influence of the liquid level to the mass-flow rate in the liquid-return hole, the initial liquid level is set as 7 mm higher than the liquid-return hole. The explanation will be introduced in Section 3.

2.3. Thermal-Physical Properties of Refrigerant and Oil

2.3.1. Density and Viscosity

As a large amount of liquid refrigerant flows into the accumulator from the evaporator during startup of the compressor, the vapor or liquid refrigerant is saturated. The density and viscosity of the refrigerant vapor in the accumulator are obtained by calling the software of NIST REFPROP 9.0 [17] based on saturated refrigerant pressure.

The liquid in the accumulator is a mixture of liquid refrigerant and oil. Both density and viscosity of the mixture are given by

$$y_{mix} = s y_{ref} + (1-s) y_{oil} \quad (3)$$

where y is the density or viscosity; s is the solubility of refrigerant in the oil. The density and viscosity of liquid refrigerant are also obtained by calling the software of NIST REFPROP 9.0, and density and viscosity of oil are calculated according to the data given by the manufacturer [18].

2.3.2. Surface Tension

The surface tension between gas and liquid has a great influence on the shape, size and speed of droplets in the accumulator, which is empirically calculated by temperature, pressure, refrigerant solubility and the surface tension of pure oil and refrigerant in the previous literature. In this paper, the surface tension of oil σ_{oil} is calculated by a linear relation between surface tension and temperature, shown as below [19].

$$\sigma_{oil} = a - bT \quad (4)$$

where σ is the surface tension, a and b are constant, as determined by experimental data.

The surface tension of the refrigerant and oil mixture is [20]:

$$\sigma_{mix} = \sigma_{ref} + (\sigma_{oil} - \sigma_{ref})\sqrt{s} \quad (5)$$

where s is the solubility of refrigerant in the oil. The subscripts "*mix*" and "*oil*" represent mixture and oil, respectively. The surface tension of refrigerant is obtained by calling the software of NIST REFPROP.

2.4. Fundamentals of CFD Method

In order to accurately predict the gas–liquid interface, the volume of fluid (VOF) models are employed to analyze the liquid-return characteristics in the accumulator. The

volume fraction of fluid component α_q can be solved by the conservation equation of volume fraction:

$$\frac{\partial}{\partial t}(\alpha_q \rho_q) + \nabla \cdot (\alpha_q \rho_q \overline{v_q}) = S_{\alpha q} + \sum_{p=1}^{n} (\dot{m}_{pq} - \dot{m}_{qp}) \tag{6}$$

where $\dot{m}_{pq}$ is the mass transfer from phase q to phase p, and $\dot{m}_{qp}$ is the mass transfer from phase p to phase q. $S_{\alpha q}$ is the source term. The primary-phase volume fraction is computed based on the following Equation (7)

$$\sum_{q=1}^{n} \alpha_q = 1 \tag{7}$$

The turbulent flow of fluid in the accumulator is a strong swirling flow due to the irregular structure and the large flow rate. The Reynolds stress model is adopted to simulate the strong swirling flow. The conservation equations of mass and momentum are

$$\frac{\partial \overline{u}_i}{\partial x_i} = 0 \tag{8}$$

$$\rho \frac{\partial \overline{u}_i}{\partial t} + \rho \overline{u}_j \frac{\partial \overline{u}_i}{\partial x_j} = \rho \overline{F}_i - \frac{\partial \overline{P}}{\partial x_i} + \frac{\partial}{\partial x_j}(\mu \frac{\partial \overline{u}_i}{\partial x_j} - \rho \overline{u'_i u'_j}) \tag{9}$$

where $\overline{u}_i$ and $\overline{u}_j$ are velocity components. $\overline{u'_i}$ and $\overline{u'_j}$ are $\overline{u'_i}$ are pulsating velocity components, $i, j = 1, 2, 3$. μ is hydrodynamic viscosity coefficient.

The k equation and ε equation are

$$\frac{\partial}{\partial t}(\rho k) + \frac{\partial}{\partial x_i}(\rho k u_i) = \frac{\partial}{\partial x_j}[(\mu + \frac{\mu_t}{\sigma_k})\frac{\partial k}{\partial x_j}] + \frac{1}{2}(P_{ii} + G_{ii}) - \rho\varepsilon(1 + 2M_1^2) + S_k \tag{10}$$

$$\frac{\partial}{\partial t}(\rho \varepsilon) + \frac{\partial}{\partial x_i}(\rho \varepsilon u_i) = \frac{\partial}{\partial x_j}[(\mu + \frac{\mu_t}{\sigma_\varepsilon})\frac{\partial \varepsilon}{\partial x_i}] + C_{\varepsilon 1}\frac{1}{2}(P_{ii} + C_{\varepsilon 3} G_{ii})\frac{\varepsilon}{k} + S_\varepsilon \tag{11}$$

where k and ε are turbulent kinetic energy and turbulence dissipation rate; μ_t is coefficient of turbulence viscosity; σ_k is turbulance Prandtl number; S_k is buoyancy source term of k equation; S_ε is buoyancy source term of ε equation; $C_{\varepsilon 1}$ and $C_{\varepsilon 3}$ are coefficients of each parameter term.

The supplementary equation of this model is the Reynolds stress-transport equation:

$$\frac{\partial}{\partial t}(\rho \overline{u'_i u'_j}) + \frac{\partial}{\partial x_i}(\rho U_k \overline{u'_i u'_j}) = D_{ij} + \varphi_{ij} + G_{ij} - \varepsilon_{ij} \tag{12}$$

where D_{ij}, φ_{ij}, G_{ij}, ε_{ij} are diffusion term, pressure-strain term, generation term and dissipation term, respectively.

The gas and liquid are immiscible. In order to identify a more obvious phase interface, the explicit volume-fraction formulation and sharp interface-modeling type is selected. The contact angle is set by default for the lack of the data of the contact angle between refrigerant gas, oil and wall in the existing literatures or practical experience. Because of the transient calculation, the pressure–velocity coupling method of PISO is selected. Geo-Restruct is selected as the discrete method of volume fraction, which can better identify the shape of the droplets. The rest are all the default settings of Fluent. The time step during calculation is adaptively adjusted, which can assure the computational stability when using the explicit formulation, and the adjustment method is Multiphase-Specific and the Global Courant Number is 2.

3. Experimental Verification

The objective of the experiment is to measure and analyze the changes of the liquid level and pressure in the accumulator during the startup process of the compressor, so as to obtain the factors influencing liquid-return characteristics in the accumulator during startup of the rotary compressor.

A schematic diagram of experimental setup is shown in Figure 5. The whole experiment was conducted in the Psychometric Rooms, which contains an indoor room and an outdoor room. It can not only provide a constant temperature and pressure environment for the experiment, but also precisely measure the capacity and power consumption of an air-conditioning system. The tested air-conditioning system consisted of a rotary compressor, an indoor heat exchanger, an outdoor heat exchanger, an expansion valve and other accessories, as shown in the figure.

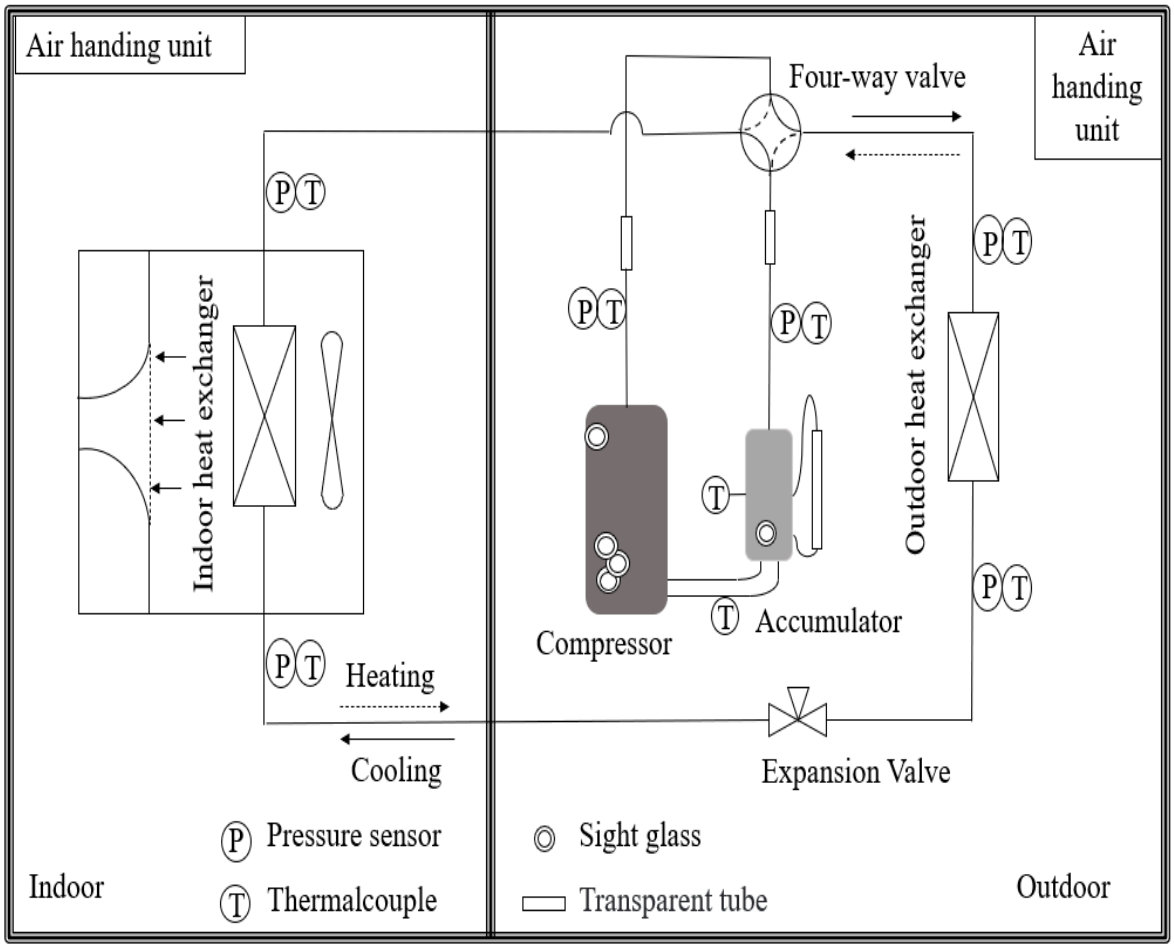

Figure 5. Schematic diagram of experimental setup.

An air conditioner (KFR-35G/BP3DN7Y-DA401 (B2)) with a two-cylinder rotary compressor produced by Midea was chosen in the test. The displacement of the compressor is 210 cm^3. As shown in Figure 5, thermocouples with accuracies of ±0.1 °C and pressure sensors with accuracies of ±0.5% FS were installed in the system to measure the temperature and pressure of the air-conditioning system.

The tested rotary compressor is shown in Figure 6. A transparent tube with a length of 15 cm was installed next to the accumulator to measure the liquid level in the accumulator, and a sight glass was installed on the accumulator shell to observe the liquid state in the accumulator. Four sight glasses used for other studies were installed on the compressor shell to observe the liquid state in the compressor. The experiment was conducted to make

sure that the sensor installation and compressor modification had little influence on the internal thermodynamic process in the compressor and its performance. The structural parameters of this accumulator are shown in Table 1.

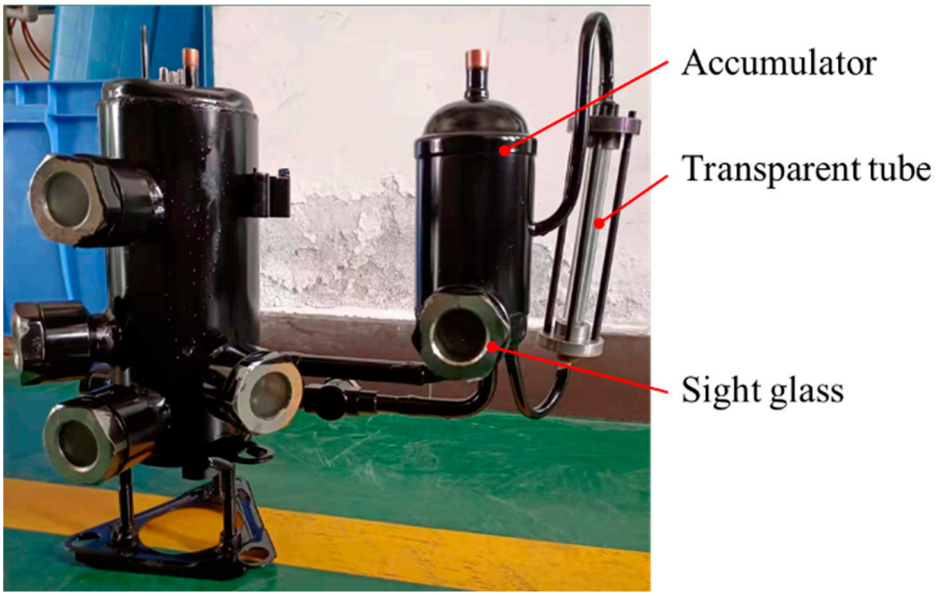

Figure 6. Test rotary compressor.

Refrigerant R290 and mineral oil were used in the air-conditioning system. The system starts at a rated frequency of 60 Hz under the heating condition with the ambient temperature of −7 °C. Before the system startup, it was placed in Psychometric Rooms for a long time to ensure that the temperature of all components and refrigerant distribution in the system were stable. The red colorant was added to the oil for easy observation.

The stable experimental results were obtained after three repetitions of the same experiment. Figure 7 shows the variations of liquid level in the accumulation during startup of the compressor. Figure 8 shows the photos of the sight glass on the accumulator shell. As shown in Figure 7, before the startup, the liquid level is equal to the height of the liquid-return holes, which can also be observed in Figure 8. After the startup, the liquid level rises rapidly and exceeds the upper limit of the sight glass because of a lot of refrigerant liquid entering the accumulator from the evaporator. Additionally, some bubbles appear on the liquid surface. The liquid level gradually drops after 100 s and disappears after 260 s. The decline in the liquid level from the peak at 95 s to the height of the liquid-return hole at 125 s is faster, because of the dual effects of the refrigerant evaporation and the outflow through the liquid-return hole. After 25 s, the liquid level is lower than the height of the liquid-return hole. The liquid refrigerant level is only reduced by evaporation, so the liquid level drops more slowly.

It can also be seen from Figure 7 that the liquid level dropped by 3.5 mm from 100 s to 110 s, and the liquid volume-flow rate through the liquid-return holes was 1.35 mL·s^{-1}. There is almost no refrigerant evaporation during this period due to no bubbles on the liquid surface. Therefore, this process was selected for numerical simulation and the evaporation of refrigerant is ignored in the calculation.

The experiment and simulation results of the volume-flow rate of the liquid flowing through the liquid-return holes are shown in the Table 2. It can be found from the table that the error between the experimental value of liquid volume-flow rate $\dot{Q}_{\mathrm{exp}}$ through the liquid-return holes and the calculated value $\dot{Q}_{cal}$ is 1.55%. This indicates that the calculation model proposed in this paper can accurately predict the liquid-return process in the accumulator during the startup of the rotary compressor. The pressure difference

between the inlet and outlet of the liquid-return hole is 10 times higher than the differential pressure due to the liquid height difference between the liquid level and the hole, so the initial liquid level is considered a negligible factor.

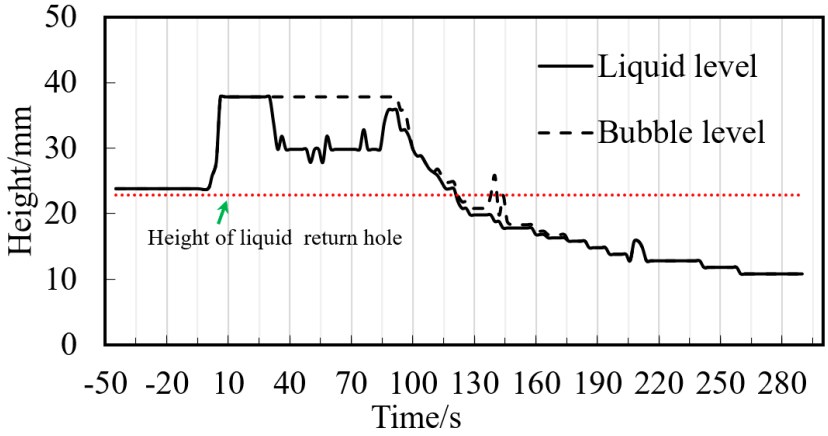

Figure 7. Variations of liquid level in the accumulation during startup.

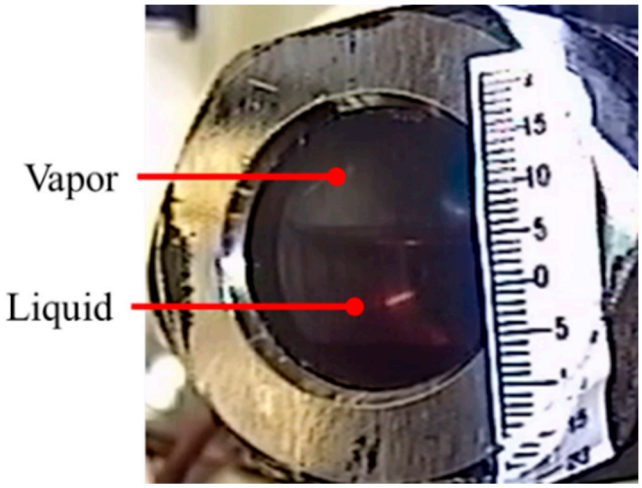

Figure 8. Photos of the sight glass on the accumulator shell before startup.

Table 2. Experiment and simulation results of liquid volume-flow rate through the liquid-return holes.

ΔH_{liqud_level}/mm	ρ_{mix}/kg·m^{-3}	ν_{mix} /mPa·s	σ_{mix} /N·m^{-1}	ΔP_{hole}/Pa	$\dot{Q}_{exp}$/mL·s^{-1}	$\dot{Q}_{cal}$/mL·s^{-1}	Errors/%
3.5	567	0.17	0.014	488	1.357	1.378	1.55

4. Results and Discussion

4.1. Effects of Refrigerant Solubility on Liquid-Return Characteristics

Under different operating conditions, the solubility of the refrigerant in the oil is different, which leads to the different thermal-physical properties of the refrigerant/oil-mixture liquid such as density, viscosity and surface tension. The difference in liquid properties has a great influence on the liquid-return characteristics of the compressor. Therefore, the average mass-flow rate and average velocity of the liquid flowing through the liquid-return holes in one compression cycle with different refrigerant solubilities are investigated. Under the same conditions as in Section 3, by varying the solubility of the refrigerant in the oil from 100% to 20%, liquid-return characteristics in the liquid-return

holes are simulated. The simulation conditions and results are shown of liquid-return characteristics in the liquid-return holes with different refrigerant solubility in Table 3.

Table 3. Liquid-return characteristics in the liquid-return holes with different refrigerant solubility.

Solubility/−	ρ_{mix}/kg·m^{-3}	ν_{mix}/mPa·s	σ_{mix}/N·m^{-1}	$\overline{m}_{mix}$/g·s^{-1}	$\overline{v}_{mix}$/m·s^{-1}
100%	567	0.17	0.014	0.781	0.390
50%	734	2.9	0.034	0.932	0.359
20%	823	68	0.039	0.445	0.153

It can be seen from the table that the viscosity of the refrigerant/oil mixture ν_{mix} increases rapidly from 0.17 mPa·s to 68 mPa·s with the decrease in solubility. The increase in liquid viscosity leads to the decline in the average mass-flow rate $\overline{m}_{mix}$ and the average liquid-return velocity $\overline{v}_{mix}$. It can also be seen from the table that as the viscosity increases by 20 times from 0.17 mPa·s to 2.9 mPa·s, the liquid-return velocity $\overline{v}_{mix}$ rises by only about 10%. The viscosity continues to increase 10 times from 2.9 mPa·s to 68 mPa·s; the liquid-return velocity $\overline{v}_{mix}$ drops by more than 2 times from 0.359 m·s^{-1} to 0.153 m·s^{-1}. This indicates that the liquid mass rate and velocity change little with a high refrigerant solubility greater than 50%.

In addition to the velocity and mass-flow rate of liquid through the liquid-return hole, the two-phase flow pattern can also be observed. Figure 9 shows the shape of the liquid flowing out of the liquid-return holes under different conditions. Due to the difference in liquid viscosity and surface tension, the liquid shape near the liquid-return hole varies greatly with the solubility. It can be seen from the figure that with the solubility of 100% and 50%, backflow bubbles appear near the liquid-return hole. Part of the liquid entering the liquid-return hole flows into the cylinder along the suction pipe wall, and the other liquid is blown and dispersed by the refrigerant vapor in the suction pipe. If the refrigerant solubility is 20%, no backflow bubbles appear near the liquid-return hole, and all liquid flows into the cylinder along the suction-pipe wall. This is because the surface tension and viscosity with the low solubility of 20% are greater than other two conditions, and the liquid has stronger cohesion and is more difficult to disperse by the gas.

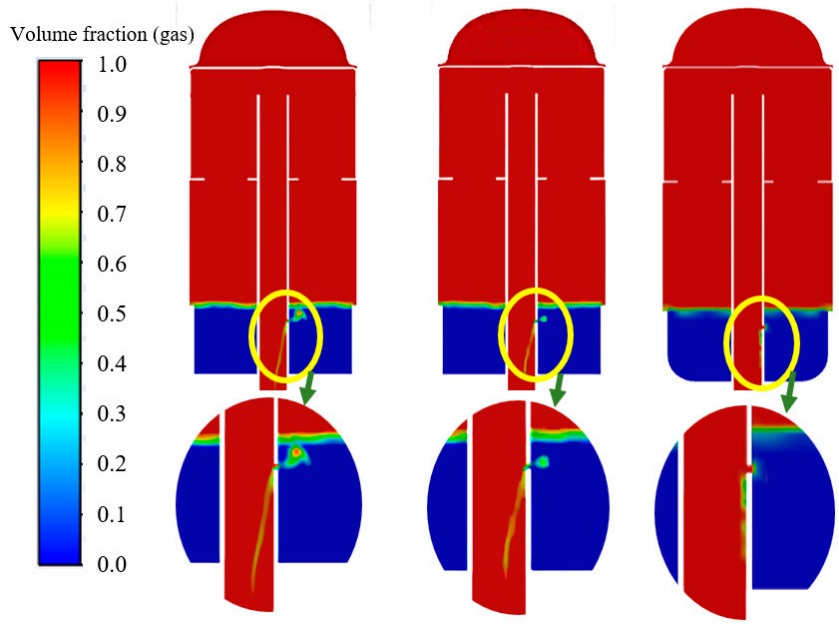

Figure 9. Shape of the liquid flowing out of the liquid-return holes. s = 100% s = 50% s = 20%.

The two-phase flow pattern in the liquid-return hole depends on the velocity vector diagram. Figure 10 shows the velocity vector diagrams. It can be seen that when the

solubility is 100% and 50%, liquid backflow occurs in the accumulator through the liquid-return hole, so a vortex will be formed in the suction pipe. When the solubility is 20%, the fluid velocity near the suction-pipe wall is almost 0, which prevents the droplets along the inner wall of the suction tube from being blown into the inside of the suction pipe.

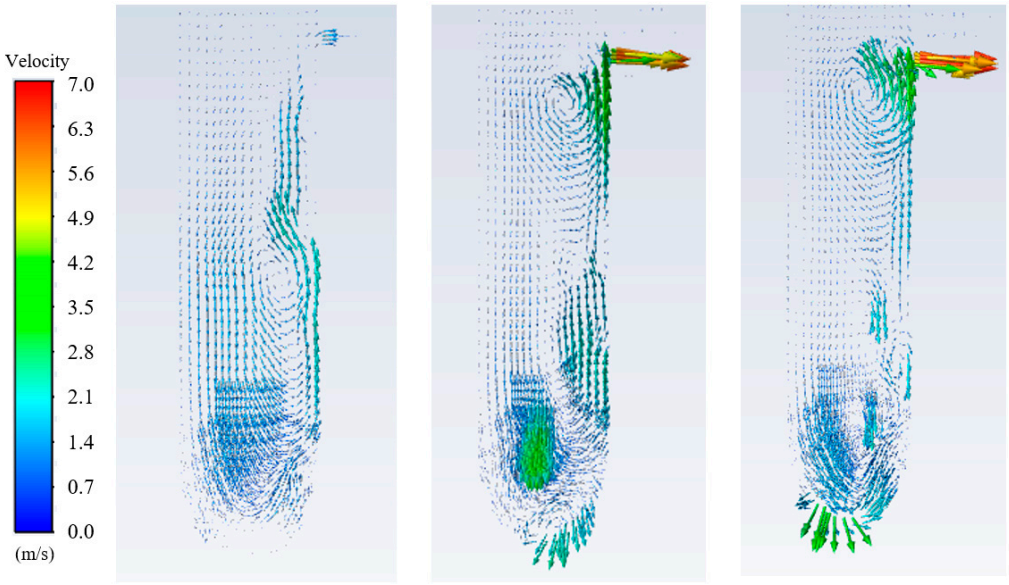

Figure 10. Velocity vector in the liquid-return hole and the suction pipe. s = 100% s = 50% s = 20%.

4.2. Effects of Refrigerant/Oil Type on Liquid-Return Characteristics

The thermal-physical properties of different refrigerants vary greatly, which would result in different liquid-return characteristics. Under the same conditions in Section 3, by using different refrigerants (R290, R22, R410A), the liquid-return characteristics in the accumulator at the refrigerant solubility of 20% is simulated. The common oils, NM56 for R22 and POE68 for R410A, are used in the simulation. The simulation conditions and results are shown in the Table 4.

Table 4. Liquid-return characteristics with different refrigerant/oil mixture.

Refrigerant/Oil	ρ_{mix}/kg·m^{-3}	ρ_g/kg·m^{-3}	ν_{mix}/mPa·s	ΔP_{hole}/Pa	$\overline{m}_{mix}$/g·s^{-1}	$\overline{v}_{mix}$/m·s^{-1}
R22/NM56	996	7.3086	39	1010	0.678	0.193
R410A/POE68	976	10.449	75	1494	0.687	0.199
R290/NM100	823	3.8324	68	706	0.445	0.153

It can be seen from Table 4 that the pressure difference between the inlet and outlet of the liquid-return hole for the R290/NM100 is 706 Pa, which is almost half of the pressure difference of R410A/POE68. Under the same suction condition, the lower density of R290 results in less pressure loss inside the accumulator, and then a smaller pressure difference between the liquid-return hole.

Besides the pressure difference on both sides, the types of refrigerant/oil also have a great influence on liquid-return velocity. It can also be seen from Table 4 that the liquid-return velocity $\overline{v}_{mix}$ of the R290/NM100 (0.153 m·s^{-1}) is much smaller than that of R22/NM56 (0.193 m·s^{-1}) and R410A/POE68 (0.199 m·s^{-1}), because of the higher liquid viscosity ν_{mix} of R290/NM100 mixture (68 mPa·s) and lower pressure difference than other two mixtures. However, because of the flammability, R290 charging in the air-conditioning is much less than other two refrigerants. This would lead to the lower R290 solubility in the accumulator than that of other two refrigerants, and then further increase the difficulty of liquid return in the accumulator during compressor startup. Therefore, the design of the liquid-return hole in

the accumulator using R290 as refrigerant should be reconsidered, such as setting multiple liquid-return holes or increasing the diameter of the liquid-return hole.

4.3. Effects of Liquid-Return-Hole Diameter on Liquid-Return Characteristics

Figure 11 shows the variations of the mass-flow rate and pressure difference in the liquid-return hole with the crank angle under different diameters' conditions. Figure 12 shows the variations of the pressure difference between two inlets and outlets of the liquid-return hole with the crank angle under different diameters' conditions. It can be seen from Figure 11 that the mass-flow rate increases with the increase in diameter under the same crank angle. The maximum mass flow is about 1.15 $g \cdot s^{-1}$ with the hole diameter D_{hole} of 2 mm at the crank angle of 120°, while it is only 0.5 $g \cdot s^{-1}$ with the hole diameter of 1 mm.

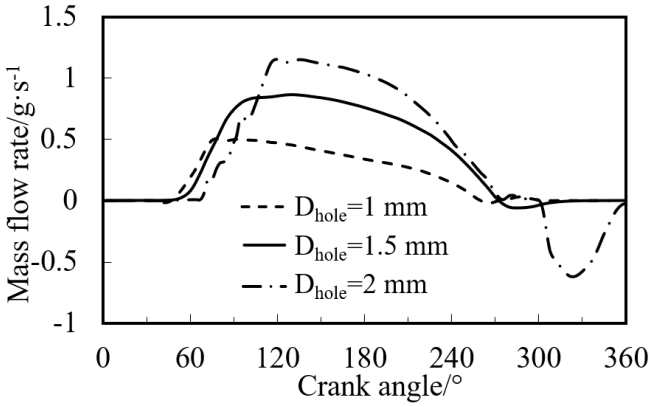

Figure 11. Variations of mass-flow rate in the liquid-return hole with the crank angle.

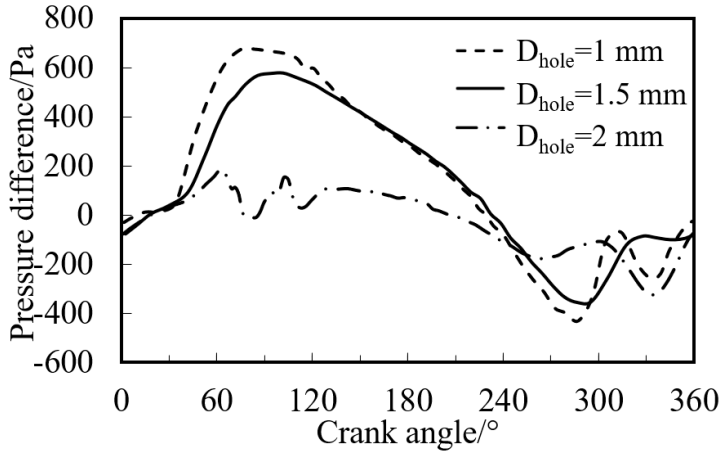

Figure 12. Variations of pressure difference with the crank angle.

It can also be observed that for the hole diameter of 2 mm, the backflow occurs after 300° of the crank angle, because the outlet pressure of the liquid-return hole is greater than the inlet pressure (see Figure 12). Although the negative pressure difference appears after 270° for all three cases, the local flow loss of a small diameter is greater than that of the large diameter, and the flow velocity is also smaller than other two cases under the same pressure difference. Therefore, the backflow for the diameter 1 mm and 1.5 mm is weak.

The liquid-return-hole diameter also affects the liquid-return velocity. Figure 13 shows the variations of liquid velocity in the liquid-return hole with the crank angle. From this figure it can be noted that the liquid velocity in the hole increases with the decrease in hole diameter. The maximum velocity for the diameter of 1 mm is 1.12 $m \cdot s^{-1}$, while the maximum velocity for the diameter of 2 mm is merely 0.64 $m \cdot s^{-1}$. This is because the pressure difference for the diameter of 1 mm or 1.5 mm is much larger than that of 2 mm

(see Figure 12). The maximum pressure difference for a hole diameter of 1 mm is 675 Pa, while for the diameter of 2 mm, the maximum pressure difference is only 181 Pa.

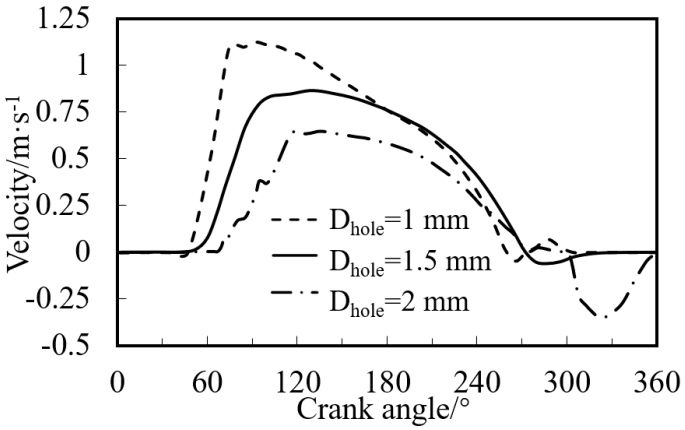

Figure 13. Variations of liquid velocity in the liquid-return hole with the crank angle.

Under the conditions of different diameters, the liquid shape in the liquid-return hole and suction pipe at the crank angle of 180° is shown in Figure 14. It can be found that for the hole diameter of 1 mm and 1.5 mm, most of the liquid flowing through the hole is dispersed by the refrigerant vapor, instead of flowing down along the suction-pipe wall. However, for the diameter of 2 mm, it can be seen that most of the liquid flows down along the suction-pipe wall, and the backflow is also observed near the hole.

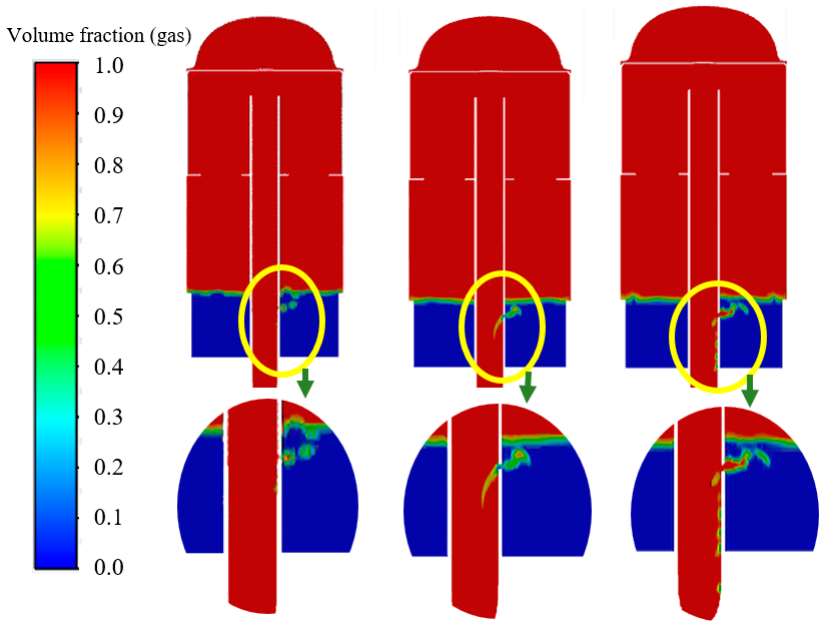

Figure 14. Liquid shape under the conditions of different liquid-return-hole diameters. D_{hole} = 1 mm D_{hole} = 1.5 mm D_{hole} = 2 mm.

4.4. Effects of Compressor Frequency on Liquid-Return Characteristics

Based on the conditions in Section 3, the mass-flow rate in the liquid-return hole in one cycle with the crank angle for different compressor frequencies is shown in Figure 15. It can be noted that there is almost no liquid flowing out of the hole at the angle of initial and final 60°. After the angle of 60°, the mass-flow rate increases with the increase in angle. After peaking at the angle of about 120°, it gradually declines. The liquid mass-flow rate is positively correlated with the compressor frequency. The backflow of the liquid, namely

negative values, near the hole occurs after the crank angle of 270° for the frequency greater than 60 Hz.

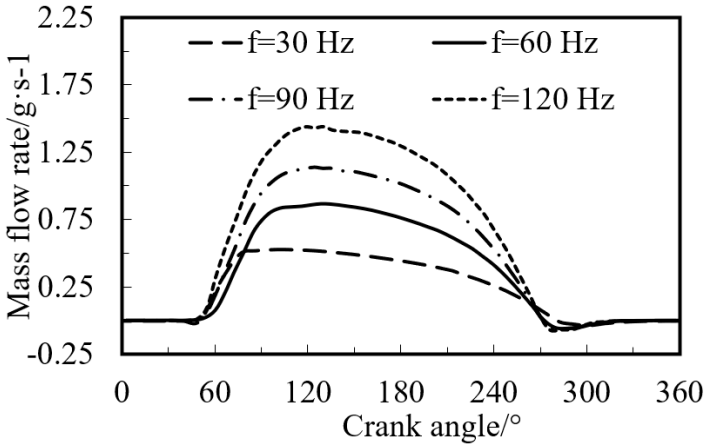

Figure 15. Variations of mass−flow rate with the crank angle for different frequencies.

The change of the frequency also affects the pressure fluctuation at the inlet and outlet of the accumulator. Figure 16a shows the pressure fluctuation at the inlet of the accumulator, and Figure 16b shows the pressure fluctuation at the outlet of the accumulator. It can be noted from the two figures that the pressure fluctuation increases with the increase in the frequency. The amplitude of pressure fluctuation at the inlet of the accumulator is smaller than that of the outlet. The maximum fluctuation value of the inlet is 3400 Pa at the frequency of 120 Hz, while it is 18,000 Pa for that of the outlet. This is because the inlet of the accumulator is farther away from the seismic source (cylinder). In addition, the inlet pressure fluctuation has only a trough at 180°, while the outlet pressure fluctuation has a trough at 90° and a peak at 300°, because the frequency of the outlet pressure fluctuation is higher than that of the inlet.

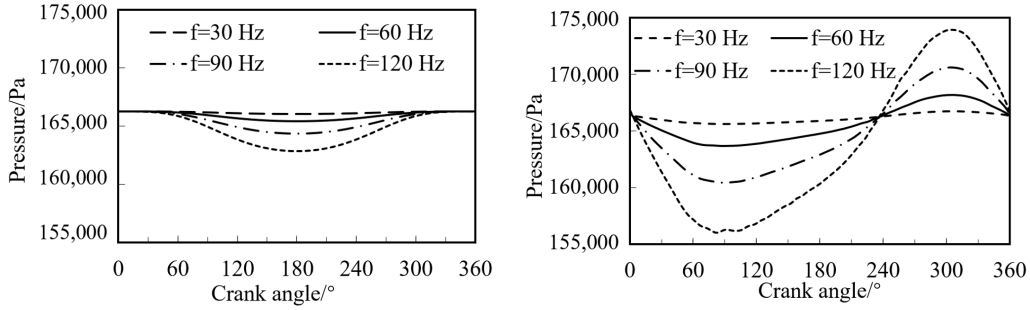

Figure 16. Pressure fluctuation of the accumulator. (**a**) inlet of the accumulator. (**b**) outlet of the accumulator.

5. Conclusions

In this paper, the numerical simulation of the liquid-return process of the accumulator during the startup of the rotary compressor is carried out. The simulation result with an error as low as 1.55% is experimentally verified. Effects of refrigerant solubility, refrigerant/oil types, liquid-return-hole diameter and compressor frequency on the liquid-return characteristics are conducted. Methods to improve the liquid-return characteristics of R290 rotary compressors are proposed. The following conclusions may be drawn:

1. During startup of the rotary compressor, the velocity and mass of the liquid flowing out of the accumulator through the liquid-return holes decrease with the decrease in refrigerant solubility in the oil. The liquid-return process is significantly slower with

the increase in surface tension and viscosity of the refrigerant/oil mixture, especially when the refrigeration solubility is less than 50%. Backflow bubbles appear near the liquid-return hole with refrigerant solubilities of 100% and 50%, while backflow bubbles appear with a low refrigerant solubility of 20%.

2. Under the same startup conditions, the liquid-return velocity and mass of the R290/NM100 mixture through the liquid-return holes in the accumulator are much smaller than those of the other two refrigerant/oil mixtures, R22/NM56 and R410A/POE68, because of the low density and high mixture viscosity for R290. Therefore, for the air-conditioning system using R290/NM100, the accumulator structure should be modified to allow more liquid to return to the compressor faster.
3. The total mass of the liquid flowing through the liquid-return hole increases with the increase in the hole diameter, but the velocity decreases instead. The mass-flow rate and velocity increase to a peak at the crank angle of 120° and then decrease gradually. With the decrease in the hole diameter, the pressure difference between the two sides of the liquid-return hole increases, and reaches a maximum value of 675 Pa at 1 mm.
4. Almost no liquid returns to the compressor at the angle of initial and final 60°, while it peaks at the angle of about 120°. With the increase in the compressor frequency, the liquid returning to the cylinder through the liquid-return holes linearly increases, but the amplitude and frequency of the pressure fluctuation at the inlet and outlet of the accumulator increase. The maximum pressure fluctuation at the outlet is 18,000 Pa with the frequency of 120 Hz.

Author Contributions: Conceptualization, J.L.; validation, J.J. and N.G.; investigation, L.H.; writing—original draft preparation, J.L; writing—review and editing, N.G.; supervision, J.W. All authors have read and agreed to the published version of the manuscript.

Funding: This research was funded by National Natural Science Foundation of China, grant number 52106019; Natural Science Foundation of Zhejiang Province, grant number LZY22E060004.

Institutional Review Board Statement: Not applicable.

Informed Consent Statement: Not applicable.

Data Availability Statement: Not applicable.

Conflicts of Interest: The authors declare no conflict of interest.

Nomenclature

A	Area (m^2)
D	Diameter (mm)
f	Frequency (Hz)
P	Pressure (Pa)
$\overline{m}$	Average mass-flow rate ($g \cdot s^{-1}$)
$\dot{Q}$	Volume-flow rate ($mL \cdot s^{-1}$)
s	Solubility(/)
u	Velocity ($m^2 \cdot s^{-1}$)-
$\overline{v}$	Average liquid velocity ($m \cdot s^{-1}$)
V	Volume (m^3)
ν	Viscosity (mPa·s)
α	Volume fraction(-)
ρ	Density($kg \cdot m^{-3}$)
θ	Crank angle(°)
η_v	Volume efficiency(−)
σ	Surface tension ($N \cdot m^{-1}$)
Subscript	
accu	Accumulato0072
c	Cylinder

m	Refrigerant/oil mixture
ref	Refrigerant
s	Suction

References

1. Lee, J.; Lee, U.Y. Design optimization of an accumulator for reducing rotary compressor noise. *Proc. Inst. Mech. Eng. Part E J. Process Mech. Eng.* **2012**, *226*, 285–296. [CrossRef]
2. Kim, M.; Park, S.; Shin, M.; Jeong, Y. Noise improvement of air conditioning accumulator using acoustic metamaterials. In Proceedings of the INTER-NOISE and NOISE-CON Congress and Conference Proceedings, Seoul, Korea, 12 October 2020.
3. Yun, K. Designing a function-enhanced suction accumulator for rotary compressor. In Proceedings of the International Compressor Engineering Conference at Purdue University, West Lafayette, IN, USA, 14 July 1998; No.1315.
4. Han, B.; Yan, G.; Yu, J. Refrigerant migration during startup of a split air conditioner in heating mode. *Appl. Therm. Eng.* **2019**, *148*, 1068–1073. [CrossRef]
5. Wang, D.; Zhang, Z.; Yu, B.; Wang, X.; Shi, J.; Chen, J. Experimental research on charge determination and accumulator behavior in trans-critical CO2 mobile air-conditioning system. *Energy* **2019**, *183*, 106–115. [CrossRef]
6. Wu, J.; Lin, J.; Zhang, Z.; Chen, Z.; Xie, J.; Lu, J. Experimental investigation on cold startup characteristics of a rotary compressor in the R290 air-conditioning system under cooling condition. *Int. J. Refrig.* **2016**, *65*, 209–217. [CrossRef]
7. Bianchi, M.; Deschamps, C.J.; Rodrigues, T.T.; Paladino, E.E. Numerical-experimental investigation of liquid slugging in the suction muffler of a hermetic reciprocating compressor. In Proceedings of the 12th International Conference on Compressors and Their Systems, London, UK, 6–8 September 2021.
8. Feng, Y.; Wu, J.; Liang, Y. Improving the start-up performance of the vapor compression cycle by recovering the lost cooling energy in the accumulator. *Appl. Therm. Eng.* **2021**, *195*, 116942. [CrossRef]
9. Kang, H.; Choi, K.; Park, C.; Kim, Y. Effects of accumulator heat exchangers on the performance of a refrigeration system. *Int. J. Refrig.* **2007**, *30*, 282–289. [CrossRef]
10. Raiser, H.; Heckenberger, T.; Tegethoff, W.; Kohler, J.; Fosterling, S. Transient behavior of R744 vehicle refrigeration cycles and the influence of the suction side accumulator design. *SAE Technical Paper*. 3 April 2006. Available online: https://saemobilus.sae.org/content/2006-01-0162/ (accessed on 1 March 2022).
11. Zhang, W.; Hrnjak, P. Modeling of an integrated internal heat exchanger and accumulator in R744 mobile air-conditioning applications. *SAE Technical Paper*. 1 April 2020. Available online: https://www.sae.org/publications/technical-papers/content/2020-01-0153/ (accessed on 1 March 2022).
12. Zhang, W.; Hrnjak, P. Numerical investigation of carbon dioxide and poe oil mixture behavior in an accumulator in trans-critical heat pump mode. In Proceedings of the 18th International Refrigeration and Air Conditioning Conference at Purdue University, West Lafayette, IN, USA, 24–28 May 2021.
13. Zheng, B.; Liang, X.; Zhuang, R. Experimental investigation on the influence of the oil return hole on the performance of R-32 wet compression cycle. In Proceedings of the 16th International Refrigeration and Air-Conditioning Conference at Purdue University, West Lafayette, IN, USA, 11–14 July 2016.
14. Lin, J.; Wu, J.; Zhang, Z.; Chen, Z.; Xie, J.; Lu, J. Experimental investigation of startup characteristics of R290 rotary compressor under low ambient temperature heating condition. *Int. J. Refrig.* **2017**, *77*, 128–135. [CrossRef]
15. Wang, C.; Wu, J.; Du, Y.; Li, J.; Du, W. Experimental study on startup characteristics of a R290 room air conditioner under various ambient temperatures. *Int. J. Refrig.* **2020**, *109*, 37–44. [CrossRef]
16. Wu, J.; Wang, G. Numerical study on oil supply system of a rotary compressor. *Appl. Therm. Eng.* **2013**, *61*, 425–432. [CrossRef]
17. Lemmon, E.W.; Huber, M.L.; McLinden, M.O. Reference fluid thermodynamic transport properties. In *NIST Standard Reference Database 23*; National Institute of Standards and Technology: Boulder, CO, USA, 2010.
18. Wu, J.; Chen, Z.; Lin, J.; Li, J. Experimental analysis on R290 solubility and R290/oil mixture viscosity in oil sump of the rotary compressor. *Int. J. Refrig.* **2018**, *94*, 24–32. [CrossRef]
19. Seeton, C.J. *Carbon Dioxide-Lubricant Two-Phase Flow Patterns in Small Horizontal Wetted Wall Channels: The Effects of Refrigerant/Lubricant Thermophysical Properties*; University of Illinois at Urbana-Champaign: Champaign, IL, USA, 2009.
20. Jensen, M.; Jackman, D. Prediction of nucleate pool boiling heat transfer coefficients of refrigerant-oil mixtures. *Heat Transf.* **1984**, *106*, 184–190. [CrossRef]